PHYSICAL REVIEW B **90**, 020402(R) (2014)

# Measuring and tailoring the Dzyaloshinskii-Moriya interaction in perpendicularly magnetized thin films

A. Hrabec,[1] N. A. Porter,[1] A. Wells,[1] M. J. Benitez,[2] G. Burnell,[1] S. McVitie,[2] D. McGrouther,[2] T. A. Moore,[1] and C. H. Marrows[1,*]

[1]*School of Physics and Astronomy, University of Leeds, Leeds LS2 9JT, United Kingdom*

[2]*School of Physics and Astronomy, University of Glasgow, G12 8QQ, United Kingdom*

(Received 17 February 2014; revised manuscript received 30 June 2014; published 16 July 2014)

We investigate the Dzyaloshinskii-Moriya interactions (DMIs) in perpendicularly magnetized thin films of Pt/Co/Pt and Pt/Co/Ir/Pt. To study the effective DMI, arising at either side of the ferromagnet, we use a field-driven domain wall creep-based method. The use of only magnetic field removes the possibility of mixing with current-related effects such as spin Hall effect or Rashba field, as well as the complexity arising from lithographic patterning. Inserting an ultrathin layer of Ir at the top Co/Pt interface allows us to access the DMI contribution from the top Co/Pt interface. We show that the insertion of a thin Ir layer leads to reversal of the sign of the effective DMI acting on the sandwiched Co layer, and therefore continuously changes the domain wall structure from the right- to the left-handed Néel wall. The use of two DMI-active layers offers an efficient way of DMI tuning and enhancement in thin magnetic films. The comparison with an epitaxial Pt/Co/Pt multilayer sheds more light on the origin of DMI in polycrystalline Pt/Co/Pt films and demonstrates an exquisite sensitivity to the exact details of the atomic structure at the film interfaces.

DOI: 10.1103/PhysRevB.90.020402 PACS number(s): 75.70.−i, 07.55.−w, 75.60.−d

The Dzyaloshinskii-Moriya interaction (DMI) [1,2] has recently returned to prominence due to recent findings in the field of magnetic domain wall (DW) motion. Initially, DWs in permalloy nanowires were widely studied [3–8], but materials with out-of-plane (OOP) anisotropy promised even higher interactions between the current and DWs [9,10]. It was subsequently shown that broken spatial symmetry plays an extremely important role in the current-induced DW propagation process in OOP materials [11–13]. However, it has been pointed out that Bloch walls, which simple magnetostatic considerations predict to be the stable DW form in such materials [14], do not have the appropriate spin texture for an efficient Slonczewski-like torque [15]. This has been demonstrated by an application of a longitudinal magnetic field which distorts the Bloch wall towards the Néel wall structure [16], leading to much more efficient DW motion [17]. This is of importance in the efficient and reliable operation of technologies such as racetrack memories [18].

Soon after this demonstration, a series of theoretical [19,20] and experimental works [21–24] showed that a magnetic field that transforms a Bloch wall into a Néel wall can exist intrinsically due to the broken inversion symmetry at the interface. This effective field arises from the DMI as a result of high spin-orbit coupling linking the broken inversion symmetry at the interface to the spin structure [25–27]. In contrast to the Heisenberg interaction (usually written as $-J\mathbf{S}_1 \cdot \mathbf{S}_2$, with $J$ being the exchange integral), which favors collinear alignment of neighboring spins $\mathbf{S}_1$ and $\mathbf{S}_2$, the DMI can be expressed as $-\mathbf{D} \cdot \mathbf{S}_1 \times \mathbf{S}_2$, thus preferring an orthogonal orientation of $\mathbf{S}_1$ and $\mathbf{S}_2$ with a given chirality depending on the direction of the DM vector $\mathbf{D}$. This interaction is equivalent to a magnetic field acting across the DW and establishes a Néel wall of fixed chirality which dictates the direction of DW motion under the influence of a spin Hall torque. This interfacial effect has been experimentally demonstrated by several *in situ* studies on epitaxial bilayers [28–30]. The DMI also plays a crucial role in bulk material systems with broken inversion symmetry, producing exotic magnetization textures such as helices or skyrmions [31,32]. Skyrmions have been created on the atomic scale using the interfacial DMI in a monolayer of Fe on Ir [33]. It has been predicted that skyrmions have a great potential for applications as magnetic memories due to their size and extremely low operational electric currents [34,35]. Therefore, finding the means for *ex situ* studies of materials with high and tunable DMIs is of a high interest.

Here we present our DMI measurements in Pt/Co/Pt and Pt/Co/Ir/Pt multilayers with variable Ir thicknesses by employing a simple magnetic-field-based method suitable for thin films with OOP magnetic anisotropy. Avoiding the use of currents to drive DW motion makes the method simple to implement, since it can be applied to sheet films and lithography is not required. Moreover, it makes the interpretation of the data much more straightforward, since the complexity of the interplay of spin-transfer, Rashba, and spin Hall torques, with their various fieldlike and Slonczewski-like components [36], does not enter the analysis. The power of magnetic-field-based techniques has been already demonstrated by observing equispeed contours in Pt/Co/Pt trilayers [37]. It has also been suggested that the detection of the Walker breakdown can be used as a direct measure of the DMI [19]. However, it is experimentally very difficult to observe the Walker breakdown field due to the fact that it is often not reached or hidden in the creep regime [38]. As will be seen below, the creep regime itself can be used to determine the strength of the DMI.

The multilayers for our study were grown by room temperature dc sputtering at base pressures $\lesssim 10^{-7}$ mbar on thermally oxidized Si substrates with a 3 nm thick Ta buffer layer. Since crystallographically ordered Pt/Ni and Ir/Ni bilayers exhibit DMIs of opposite sign [30], the effective DMI in the Co

*c.h.marrows@leeds.ac.uk

 

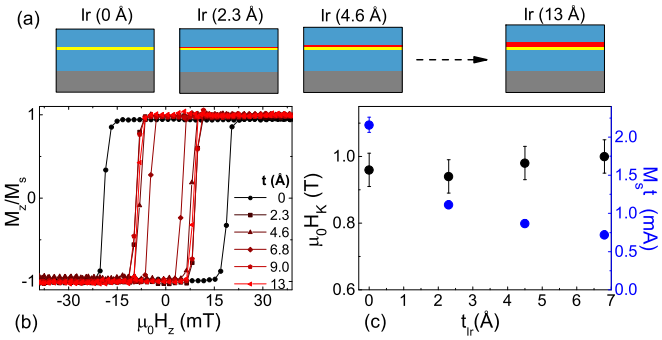


FIG. 1. (Color online) (a) Sketch of the studied Ta/Pt/Co/Ir($t_{\mathrm{Ir}}$)/Pt layer stacks with a varying Ir thickness. (b) Polar Kerr hysteresis loops for samples with various Ir thicknesses. (c) Anisotropy field $\mu_0 H_{\mathrm{K}}$ and areal magnetization $M_s t$ as a function of $t_{\mathrm{Ir}}$.

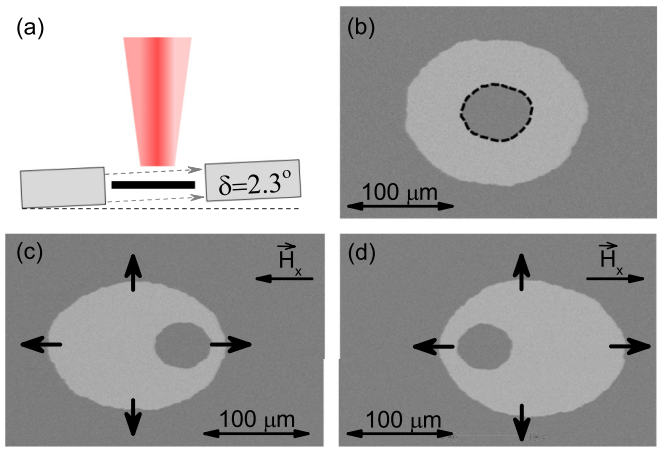


FIG. 2. (Color online) (a) Experimental setup in the Kerr microscope for DMI measurement. The magnetic field is tilted by an angle $\delta$ with respect to the sample plane. (b) DW displacement in the case of $\delta = 90^\circ$ after the application of a 1 s and $\mu_0 H_z = 7$ mT pulse. The initial DW position is indicated by the dashed line. (c) DW displacement in the case of $\delta = 2.3^\circ$ after the application of a 1 s and $\mu_0 H_x = +60$ mT pulse. (d) DW displacement after the application of a magnetic field pulse of the same length and $\mu_0 H_x = -60$ mT. Black arrows indicate the equilibrium orientation of the magnetic moments within the DW.

layer can be potentially enhanced by placing the Pt and Ir layers on either side, i.e., using two DMI-active layers. In order to reveal the effect of an Ir interface, we started from a stack of Pt(5 nm)/Co(0.7 nm)/Pt(3 nm) and inserted a thin layer of various Ir thicknesses $t_{\mathrm{Ir}}$ at the interface between the Co and top Pt layer, as depicted in Fig. 1(a). All the films exhibit a perpendicular anisotropy, as shown by the square OOP hysteresis loops presented in Fig. 1(b). The coercive field of about 20 mT in Pt/Co/Pt drops to about 9 mT as soon as the top surface is dusted with any thickness of Ir. The OOP anisotropy was measured by the vibrating sample magnetometry technique in an in-plane field configuration. Figure 1(c) shows that the anisotropy field $\mu_0 H_{\mathrm{K}}$ is about 1 T for all the films, which demonstrates that the anisotropy comes mostly from the bottom Pt/Co interface [39]. This is experimentally convenient, since it permits us to study changes in the DMI from the inclusion of the Ir layer without the complication of varying OOP anisotropy—and quantities that depend on it such as DW width—also varying.

The field-induced DW displacement was investigated by Kerr microscopy in the polar configuration. Due to its depth sensitivity it is appropriate for determining the DMI in buried layers or films adapted to real devices. The experimental setup is shown in Fig. 2(a). The magnetic field was applied in plane with a small out-of-plane component necessary to move the DW. This is achieved by tilting the magnet by an angle $\delta$ with respect to the sample plane. The role of the in-plane field is demonstrated in Figs. 2(b)–2(d). In each case, a reverse domain was nucleated and allowed to expand a little before switching off the field. Its shape was then recorded, indicated by the dashed line shown in Fig. 2(b). Consequently, we applied a 0.8–120 s long pulse of a magnetic field up to 350 mT, during which the domain expands as the DW propagates outwards. In the case of an OOP field, i.e., $\delta = 90^\circ$, the domain expansion is homogeneous [Fig. 2(b)]. The situation was very different in the case of an in-plane field component when $\delta \approx 2.3^\circ$, as shown in Fig. 2(c). One can immediately see that the DWs moving to the left and to the right moved with different velocities while the DWs moving in the directions perpendicular to the in-plane field moved with the same velocities. Our explanation for this observation is that the magnetic film contains Néel walls rather than Bloch walls. The in-plane magnetic field thus breaks the symmetry, and the magnetic moments within the DW on the right would be initially antiparallel, whereas the ones on the left parallel, to the magnetic field. To confirm this hypothesis, we have reversed the sense of the in-plane magnetic field [Fig. 2(d)].

We investigated systematically the DW velocities in the direction of in-plane magnetic field as a function of field pulse strength. A representative picture of the DW motion in a Pt/Co/Pt film is shown in Fig. 3(a), showing the right-hand DW moving much faster than the left-hand one for a left pointing in-plane field component. We emphasize that the DW creep is driven by the small OOP component and the in-plane field component breaks the radial symmetry of the creep velocity. This is expressed by the asymmetry of the velocity-field curves in Fig. 3(d). The detected asymmetry almost disappears in the film with 2.3 Å of Ir [Fig. 3(b)], and has the opposite sign in the samples with no Ir [Fig. 3(a)] and 4.6 Å of Ir [Fig. 3(c)]. The corresponding curves in Fig. 3(d) reflect these asymmetries. The inverted asymmetry suggests an inversion of the spin texture within the DWs.

The DW displacement at low magnetic fields follows the creep law [38], which can be expressed as

$$v = v_0 \exp[-\zeta(\mu_0 H_z)^{-\mu}], \tag{1}$$

where $\mu = 1/4$ is the creep scaling exponent, $v_0$ is the characteristic speed, and $\zeta$ is the scaling coefficient, which can be expressed as [37]

$$\zeta = \zeta_0[\sigma(H_x)/\sigma_0]^{1/4}, \tag{2}$$

where $\zeta_0$ is a scaling constant and $\sigma$ is the DW energy density, which is dependent on the in-plane magnetic field $\mu_0 H_x$ [19].

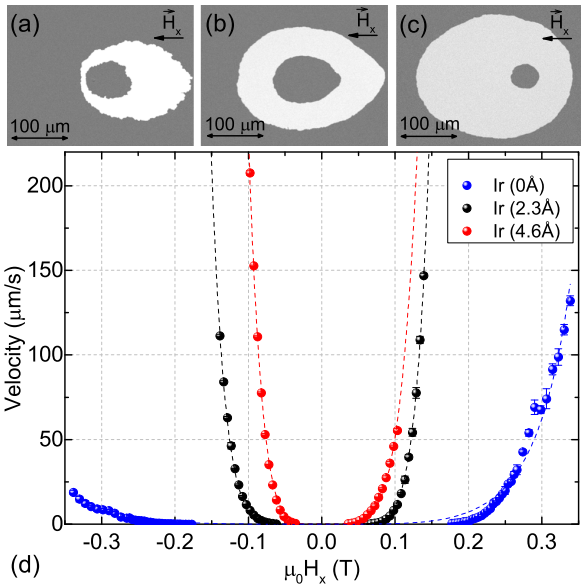


FIG. 3. (Color online) Differential Kerr image of the DW displacement in the case of (a) Ir (0 Å), (b) Ir (2.3 Å), and (c) Ir (4.6 Å) after the application of a 1 s and 320 mT, 1 s and 130 mT, and 5 s and 60 mT field pulse, respectively. (d) DW velocity as a function of in-plane magnetic field $H_x$ in the case of Ir (0 Å), Ir (2.3 Å), and Ir (4.6 Å) for a DW creeping along the $x$ direction. The remanent field in $H_x$ is smaller than 1 mT. The dashed curves show the fits of the creep model described by Eq. (1) to the data.

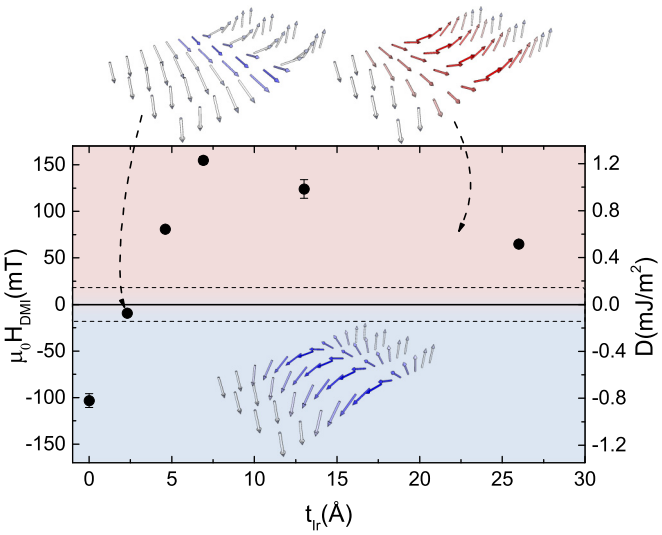


FIG. 4. (Color online) DM field and $D$ as a function of Ir thickness. The region between two dashed lines depicts the range where the DW structure changes continuously from a Néel wall to a Bloch wall and to a Néel wall of opposite chirality. Below this line (blue area) the right-handed Néel wall is stable whereas above this line (red area) it is the left-handed Néel wall. The wall structures are depicted with sketches.

This dependence can be written as

$$\sigma(H_x) = \sigma_0 - \frac{\pi^2 \Delta \mu_0^2 M_s^2}{8K_D}(H_x + H_{DMI})^2 \qquad (3)$$

for the case when the combination of the external magnetic field $\mu_0 H_x$ and the intrinsic DM field $\mu_0 H_{DMI}$ is not able to fully transform the Bloch wall into the Néel wall, i.e., $|H_x + H_{DMI}| < 4K_D/\pi\mu_0 M_s \equiv \mu_0 H_{N-B}$ and

$$\sigma(H_x) = \sigma_0 + 2K_D\Delta - \pi\Delta\mu_0 M_s|H_x + H_{DMI}| \qquad (4)$$

in the case of the Néel wall. In these expressions, $M_s$ is the saturation magnetization, $\sigma_0$ is the Bloch wall energy density, $K_D$ is the DW anisotropy energy density, and $\Delta$ is the DW width. In this model we use $M_s = 1.1 \times 10^6$ A/m$^2$, $A = 16$ pJ/m, $K_0 = \mu_0(H_K M_s - M_s^2/2) = 3.4 \times 10^5$ J/m$^3$, $\Delta = \sqrt{A/K_0} = 7.2$ nm, and $\sigma_0 = 2\pi\sqrt{AK_0} = 14$ mJ/m$^2$. The magnetostatic shape anisotropy term favoring the Bloch wall $K_D = N_x\mu_0 M_s^2/2 = 1.7 \times 10^4$ J/m$^3$, where $N_x$ is the demagnetizing coefficient of the wall [40]. As such, this model only requires three fitting parameters that are not determined by other experiments: the scaling parameters $v_0$ and $\zeta_0$, and $H_{DMI}$ itself. This symmetry-breaking term is thus solely responsible for the asymmetry in the velocity-magnetic field plots.

This model was fitted to the data for all our samples, with the fitted curves shown as the dashed lines in Fig. 3(d), and the model can be seen to give an excellent description of the experimental results. The validity of the creep law has also been confirmed by another experimental setup [41]. The extracted DM fields as a function of Ir thickness are displayed in Fig. 4. One can see that the DM field sign reversal qualitatively agrees with the asymmetry reversal shown in Figs. 3(a)–3(c). The DM field is large and negative in the Pt/Co/Pt film, nearly compensated in the case of 2.3 Å of Ir and positive for $t_{Ir}$ of 4.6 Å or greater. The calculated critical field separating the Néel wall stability region from the Bloch-Néel wall transition region is $|\mu_0 H_{N-B}| \approx 18$ mT. When $H_{DMI} < -H_{N-B}$, the DMI is able to stabilize the Néel wall structure of right-handed chirality, while for $H_{DMI} > +H_{N-B}$ the stable structure is the left-handed Néel wall, as depicted in Fig. 4. The region between the two dashed lines denotes the transition region in which the DW is continuously distorted from the pure Bloch wall towards the Néel walls of the appropriate chirality (a closer insight into the DW behavior in this region is illustrated by the micromagnetic calculations [41]). This behavior is similar to the one observed in epitaxially grown films by Chen *et al.* [30], where the DM constant reverses sign on a similar length scale upon insertion of a thin Ir interlayer. We also emphasize that the suggested DW structure depicted in Fig. 2 is no longer valid during the magnetic field pulse and all the magnetic moments eventually reorient into the field direction for sufficiently high magnetic fields. Such DWs, despite the similar magnetic moment orientation, have different energies expressed by Eq. (4), resulting in different velocities in the creep regime.

We also estimate the effective DM constant $D$ by using the expression $D = \mu_0 H_{DMI} M_s \Delta$ [19]. This is given on the right-hand ordinate axis of Fig. 4. It is apparent that the DMI in these samples is controlled largely by the top interface, in contrast to the OOP anisotropy, which we saw above to be dominated by the bottom interface. The strongest DMI, $D = 1.2 \pm 0.1$ mJ/m$^2$, is obtained in the case of Pt/Co/Ir, which can be compared to the critical DMI $D_{crit}$, resulting

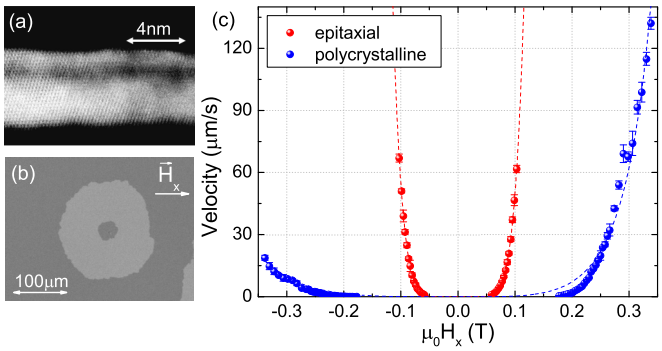


FIG. 5. (Color online) (a) High-angle annular dark field in a scanning transmission electron micrograph of the epitaxial Pt(3 nm)/Co(0.7 nm)/Pt(1 nm) trilayer. The darker Co layer is sandwiched between the two brighter Pt layers. (b) Differential Kerr image of the DW displacement in the epitaxial Pt/Co/Pt sample after the application of a 1 s long, $\mu_0 H_x = 100$ mT field pulse. (c) Comparison of DW velocities as a function of magnetic field in the polycrystalline and epitaxial films. The dashed curves show the fits of the creep model described by Eq. (1).

in a nonuniform magnetization state such as a cycloidal or skyrmionic phase. The critical DM constant can be estimated by using $D_{\text{crit}} = 4/\pi\sqrt{AK_0}$ [42], which in this case is $D_{\text{crit}} \sim 3$ mJ/m$^2$. However, the case of $D < D_{\text{crit}}$ is very important for applications due to the coexistence of ferromagnetic and skyrmionic phases, so that isolated skyrmions can be used for information encoding [34].

A strong DMI is also measured in the most structurally symmetric sample of Pt/Co/Pt, where one would not expect any DMI at all. In order to understand the origin of the strong DMI in the stack of Pt/Co/Pt, we grew a similar stack of Pt(3 nm)/Co(0.7 nm)/Pt(1 nm) epitaxially. The seed Pt layer was grown by the sputtering technique directly on a C-plane sapphire substrate at 500 °C followed by the Co/Pt bilayer sputtering at 100 °C, as described in Ref. [43]. The epitaxial character of the grown film was confirmed by x-ray diffraction and high-angle annular dark-field imaging in a scanning transmission electron microscope. Figure 5(a) shows the high level of crystallographic ordering in the epitaxial trilayer. In order to study the DMI we have performed the same measurements as described above and Fig. 5(b) shows a representative DW displacement for the epitaxial sample. One can directly see the striking difference from the picture obtained on the polycrystalline Ta/Pt/Co/Pt sample that was shown in Fig. 3(a). The observed asymmetry is in this case suppressed and the DW displacement becomes radially symmetric. This is also expressed by the symmetric velocity-field curve shown in Fig. 5(c), resulting in $D = 0.02 \pm 0.01$ mJ/m$^2$. The effective DMI thus vanishes in the case of the crystallographically symmetric interfaces on either side of the ferromagnet, just as expected. An important conclusion from the demonstrated experiment is that the DMI shows exquisite sensitivity to the atomic-scale details of the interfacial structure in these kinds of multilayer. Nevertheless, characterizing the details of potentially asymmetric interface properties, such as the roughness, degree of intermixing, and density of stacking faults, remains an outstanding materials science challenge.

Besides the asymmetric metal composition and crystallographic structure around the ferromagnetic layer, the asymmetrically induced magnetic moment may play an important role. It has been shown that Pt and Ir exhibit a strong proximity effect in the vicinity of a ferromagnet [44], and therefore one would expect different induced magnetic moments on either side of the Co layer. In our magnetometry data shown in Fig. 1(c) we see a significant drop of normalized magnetization once the Ir layer is inserted between the top Co/Pt interface. The effect of this asymmetry on the DMI is not yet fully understood [45].

In conclusion, we have demonstrated and quantified the role of an inserted thin Ir film in sputtered Pt/Co/Ir/Pt layers. We are able to control the DW chirality by changing the thickness of the Ir film via an inversion of the effective intrinsic DM field. We also reveal the crucial importance of the exact nature of the ferromagnet/heavy metal interface for the DMI by comparing a polycrystalline multilayer of the type studied in most laboratories to a similar multilayer with controlled crystallographic order. The use of two DMI-active layers opens the way for the DMI enhancement in multilayer structures intended for use in DW and skyrmion racetrack memories.

This work was supported by the U.K. EPSRC (Grants No. EP/I011668/1, No. EP/I013520/1, No. EP/K003127/1, and No. EP/J007110/1), the Scottish Universities Physics Alliance, and the University of Glasgow. The authors thank Stefania Pizzini for helpful discussion.

[1] I. Dzyaloshinsky, J. Phys. Chem. Solids **4**, 241 (1958).
[2] T. Moriya, Phys. Rev. **120**, 91 (1960).
[3] L. Gan, S. H. Chung, K. H. Aschenbach, M. Dreyer, and R. D. Gomez, IEEE Trans. Magn. **36**, 3047 (2000).
[4] M. Kläui, C. A. F. Vaz, J. A. C. Bland, W. Wernsdorfer, G. Faini, E. Cambril, L. J. Heyderman, F. Nolting, and U. Rüdiger, Phys. Rev. Lett. **94**, 106601 (2005).
[5] A. Yamaguchi, T. Ono, S. Nasu, K. Miyake, K. Mibu, and T. Shinjo, Phys. Rev. Lett. **92**, 077205 (2004).
[6] M. Hayashi, L. Thomas, C. Rettner, R. Moriya, and S. S. P. Parkin, Nat. Phys. **3**, 21 (2006).
[7] G. Meier, M. Bolte, R. Eiselt, B. Krüger, D. H. Kim, and P. Fischer, Phys. Rev. Lett. **98**, 187202 (2007).
[8] S. Lepadatu, A. Vanhaverbeke, D. Atkinson, R. Allenspach, and C. H. Marrows, Phys. Rev. Lett. **102**, 127203 (2009).
[9] O. Boulle, J. Kimling, P. Warnicke, M. Kläui, U. Rüdiger, G. Malinowski, H. J. M. Swagten, B. Koopmans, C. Ulysse, and G. Faini, Phys. Rev. Lett. **101**, 216601 (2008).
[10] L. San Emeterio Alvarez, K.-Y. Wang, S. Lepadatu, S. Landi, S. J. Bending, and C. H. Marrows, Phys. Rev. Lett. **104**, 137205 (2010).
[11] T. A. Moore, I. M. Miron, G. Gaudin, G. Serret, S. Auffret, B. Rodmacq, A. Schuhl, S. Pizzini, J. Vogel, and M. Bonfim, Appl. Phys. Lett. **93**, 262504 (2008).
[12] I. M. Miron, G. Gaudin, S. Auffret, B. Rodmacq, A. Schuhl, S. Pizzini, J. Vogel, and P. Gambardella, Nat. Mater. **9**, 230 (2010).

[13] L. Liu, C.-F. Pai, Y. Li, H. W. Tseng, D. C. Ralph, and R. A. Buhrman, Science **336**, 555 (2012).
[14] A. Malozemoff and J. Slonczewski, *Magnetic Domain Walls in Bubble Materials* (Academic, New York, 1979).
[15] A. V. Khvalkovskiy, V. Cros, D. Apalkov, V. Nikitin, M. Krounbi, K. A. Zvezdin, A. Anane, J. Grollier, and A. Fert, Phys. Rev. B **87**, 020402(R) (2013).
[16] P. P. J. Haazen, E. Murè, J. H. Franken, R. Lavrijsen, H. J. M. Swagten, and B. Koopmans, Nat. Mater. **12**, 299 (2013).
[17] E. Martinez, S. Emori, and G. S. D. Beach, Appl. Phys. Lett. **103**, 072406 (2013).
[18] S. S. P. Parkin, M. Hayashi, and L. Thomas, Science **320**, 190 (2008).
[19] A. Thiaville, S. Rohart, E. Jué, V. Cros, and A. Fert, Europhys. Lett. **100**, 57002 (2012).
[20] K.-W. Kim, H.-W. Lee, K.-J. Lee, and M. D. Stiles, Phys. Rev. Lett. **111**, 216601 (2013).
[21] S. Emori, U. Bauer, S.-M. Ahn, E. Martinez, and G. S. D. Beach, Nat. Mater. **12**, 611 (2013).
[22] K.-S. Ryu, L. Thomas, S.-H. Yang, and S. S. P. Parkin, Nat. Nanotechnol. **8**, 527 (2013).
[23] O. J. Lee, L. Q. Liu, C. F. Pai, Y. Li, H. W. Tseng, P. G. Gowtham, J. P. Park, D. C. Ralph, and R. A. Buhrman, Phys. Rev. B **89**, 024418 (2014).
[24] J. Torrejon, J. Kim, J. Sinha, S. Mitani, M. Hayashi, M. Yamanouchi, and H. Ohno, arXiv:1401.3568.
[25] A. R. Fert, Mater. Sci. Forum **59-60**, 439 (1991).
[26] A. Crépieux and C. Lacroix, J. Magn. Magn. Mater. **182**, 341 (1998).
[27] F. Freimuth, S. Blügel, and Y. Mokrousov, J. Phys.: Condens. Matter **26**, 104202 (2014).
[28] O. Pietzsch, A. Kubetzka, M. Bode, and R. Wiesendanger, Phys. Rev. Lett. **92**, 057202 (2004).
[29] M. Bode, M. Heide, K. von Bergmann, P. Ferriani, S. Heinze, G. Bihlmayer, A. Kubetzka, O. Pietzsch, S. Blügel, and R. Wiesendanger, Nature (London) **447**, 190 (2007).
[30] G. Chen, T. Ma, A. T. N'Diaye, H. Kwon, C. Won, Y. Wu, and A. K. Schmid, Nat. Commun. **4**, 2671 (2013).
[31] U. K. Rößler, A. N. Bogdanov, and C. Pfleiderer, Nature (London) **442**, 797 (2006).
[32] N. Nagaosa and Y. Tokura, Nat. Nanotechnol. **8**, 899 (2013).
[33] S. Heinze, K. von Bergmann, M. Menzel, J. Brede, A. Kubetzka, R. Wiesendanger, G. Bihlmayer, and S. Blügel, Nat. Phys. **7**, 713 (2011).
[34] J. Sampaio, V. Cros, S. Rohart, A. Thiaville, and A. Fert, Nat. Nanotechnol. **8**, 839 (2013).
[35] J. Iwasaki, M. Mochizuki, and N. Nagaosa, Nat. Nanotechnol. **8**, 742 (2013).
[36] K. Garello, I. M. Miron, C. O. Avci, F. Freimuth, Y. Mokrousov, S. Blügel, S. Auffret, O. Boulle, G. Gaudin, and P. Gambardella, Nat. Nanotechnol. **8**, 587 (2013).
[37] S.-G. Je, D.-H. Kim, S.-C. Yoo, B.-C. Min, K.-J. Lee, and S.-B. Choe, Phys. Rev. B **88**, 214401 (2013).
[38] P. J. Metaxas, J. P. Jamet, A. Mougin, M. Cormier, J. Ferré, V. Baltz, B. Rodmacq, B. Dieny, and R. L. Stamps, Phys. Rev. Lett. **99**, 217208 (2007).
[39] D. Lacour, M. Hehn, M. Alnot, F. Montaigne, F. Greullet, G. Lengaigne, O. Lenoble, S. Robert, and A. Schuhl, Appl. Phys. Lett. **90**, 192506 (2007).
[40] S. V. Tarasenko, A. Stankiewicz, V. V. Tarasenko, and J. Ferré, J. Magn. Magn. Mater. **189**, 19 (1998).
[41] See Supplemental Material at http://link.aps.org/supplemental/10.1103/PhysRevB.90.020402 for domain wall creep model and micromagnetic simulations.
[42] M. Heide, G. Bihlmayer, and S. Blügel, Phys. Rev. B **78**, 140403 (2008).
[43] A. P. Mihai, A. L. Whiteside, E. J. Canwell, C. H. Marrows, M. J. Benitez, D. McGrouther, S. McVitie, S. McFadzean, and T. A. Moore, Appl. Phys. Lett. **103**, 262401 (2013).
[44] G. Schütz and P. Fischer, Z. Phys. A: Hadrons Nucl. **341**, 227 (1992).
[45] K.-S. Ryu, S.-H. Yang, L. Thomas, and S. S. P. Parkin, Nat. Commun. **5**, 3910 (2014).